TECHNICAL ARTICLE

Applications of Rietveld-based QXRD analysis in mineral processing

Jian Li,[1,a] Robbie G. McDonald,[1] Anna H. Kaksonen,[2] Christina Morris,[2] Suzy Rea,[2] Kayley M. Usher,[2] Jason Wylie,[2] Felipe Hilario,[3] and Chris A. du Plessis[3]
[1]*CSIRO Mineral Resources Flagship, 7 Conlon Street, Waterford, WA 6152, Australia*
[2]*CSIRO Land and Water Flagship, 147 Underwood Avenue, Floreat, WA 6014, Australia*
[3]*Vale, Mineral Projects and Technology Department, BR381 Km 450, Distrito Industrial Simão, da Cunha – Santa Luzia, Minas Gerais, Brazil*

(Received 3 September 2014; accepted 30 September 2014)

Rietveld-based quantitative X-ray diffraction (QXRD) has been extensively used for mineralogical characterization in order to understand the reaction chemistry, and kinetics of minerals leaching and formation. This work presents examples where QXRD has been applied to understanding fundamental aspects of these two processes. Firstly, the co-processing of nickel laterites and sulphidic materials has the potential to offer several advantages that include the use of lower grade (including non-smeltable) concentrates, improvement in the rheological behaviour of the blends, and reduction in the use of sulphuric acid. The leaching kinetics and chemistry of mixed nickel laterite ore and sulphide concentrate were explored by the QXRD analysis of feed materials and, intermediates and final leach residues produced using controlled oxidation rates. Under high temperature (250 °C) and pressure oxidation (~40 to 45 atm.) conditions, sulphide minerals in the nickel concentrate underwent several oxidative hydrothermal transformations, and ferrous iron was oxidized and precipitated primarily as hematite. High recovery of nickel can be achieved with low acid consumption under these conditions. Secondly, iron precipitation/removal is an important down-stream process in hydrometallurgy. Moderate concentrations of ferrous iron can be oxidized using micro-organisms with oxidation rates several orders of magnitude faster compared with abiotic oxidation at ambient temperature and pressure. QXRD and chemical analysis have indicated that after oxidation, iron at pH ~2 mostly precipitates as jarosite with various amounts of K^+, Na^+, NH_4^+, and H_3O^+ incorporated into the structure. Bio-catalysed iron removal can be achieved with minimum copper and nickel losses at relatively low pH conditions.
[doi:10.1017/S0885715614001134]

Key words: nickel laterite, nickel sulphide, co-processing, bio-oxidation, jarosite, QXRD

I. INTRODUCTION

Rietveld-based quantitative X-ray diffraction (QXRD) allows an accurate estimation of changes in the mineralogical composition of solids or slurries. The application of QXRD analysis has been used extensively in research of hydrometallurgical processes, particularly the reaction chemistry and kinetics of ore leaching (Scarlett *et al.*, 2008; Wang *et al.*, 2011, 2014). The formation of new phases as a result of precipitation is often encountered during ore leaching processes, especially under high-temperature conditions, and the formation of these phases can be monitored by the QXRD analysis (Whittington *et al.*, 2003b; Madsen *et al.*, 2005). In this work, two case studies are discussed to demonstrate how Rietveld-based QXRD can be applied to improve understandings of ore processing and mineral formation.

Case One: Nickel laterites contain ~70% of the world's land-based nickel resources, whereas sulphides contain the remaining ~30% (Dalvi *et al.*, 2004). With the rapid depletion of the nickel sulphide resources, global production of nickel from laterite ores has increased from 42% in 2003 (Dalvi *et al.*, 2004) to ~56% in 2012, overtaking the production from sulphide ores. Western Australia (WA) hosts approximately 90% of the total Australian economic nickel resources (Geoscience Australia, 2012). Some of the laterite ore which deposits in WA are located in the close proximity to sulphide ore deposits, offering a potential opportunity for the co-processing of oxidic and sulphidic materials (Quinn *et al.*, 2009). Traditionally high-pressure acid leaching (HPAL) has been commercially applied to nickel laterite ores (Whittington and Muir, 2000). In co-processing, nickel laterite and sulphidic materials (e.g. nickel sulphide concentrates) are mixed and processed under HPAL conditions (McDonald *et al.*, 2012). This blending can improve the rheology of the pulp as compared with laterite ore processing (Rodriguez, 2009), with addition of an oxidant enabling *in situ* sulphuric acid production with co-generation of heat, improving overall nickel recovery and, potentially enabling the processing of "dirty" concentrates (e.g. containing As, Sb, and Hg) and concentrates obtained from disseminated sulphide ores (McDonald *et al.*, 2012). The reaction chemistry during co-processing is complex and not well understood, and the aim of the current study was to better understand the oxidation of the sulphide minerals. Changes to the iron hydrolysis chemistry during co-processing were also investigated.

[a]Author to whom correspondence should be addressed. Electronic mail: jian.li@csiro.au

Case Two: Solutions rich in ferrous iron (Fe^{2+}) are generated during oxidative leaching of sulphide ores and reductive leaching of oxide ores (Ozkaya *et al.*, 2007; Nurmi *et al.*, 2009; du Plessis *et al.*, 2011). The subsequent oxidation of Fe^{2+} to ferric iron (Fe^{3+}) and precipitation of Fe^{3+} from the leach solutions are required to remove excess iron that can passivate mineral surfaces and interfere with valuable metals recovery. Biologically catalysed Fe^{2+} oxidation is preferred over abiotic oxidation, as it is several orders of magnitude faster than abiotic oxidation at low pH (Rawlings, 2002). In this study, a two-stage reactor configuration recently proposed by du Plessis *et al.* (2011) was used for biological Fe^{2+} oxidation and subsequent Fe^{3+} precipitation as jarosite. The aim of this work was to use QXRD to confirm the formation of jarosite, to determine the crystallinity, and the incorporation of cations in the jarosite structure.

II. EXPERIMENTAL

A. Materials and methods

Case One: Details of the materials and experimental procedures can be found elsewhere (McDonald *et al.*, 2012). Briefly, the nickel laterite ore, obtained from the Bulong complex, 40 km east of Kalgoorlie in WA, was ball milled and wet screened to $-500\,\mu$m. A Poseidon nickel concentrate sample was dry screened to $-75\,\mu$m. Tests using just the Poseidon nickel sulphide concentrate were run using 10% (w/w) pulp density, whereas those with only Bulong nickel laterite employed 30% (w/w) pulp density. For blends of Bulong nickel laterite with Poseidon nickel concentrate, the ratio of concentrate to laterite was calculated, so that sufficient *in situ* sulphuric acid was formed to leach the laterite ore. A series of feeds were leached at 250 °C using a 1 gal. Parr titanium autoclave and Poseidon site process the water (Na^+ 3.1, K^+ 0.08, Mg^{2+} 0.33, Ca^{2+} 0.11, SO_4^{2-} 0.89, Cl^- 5.3, g l^{-1}). The oxidation of the concentrate was enabled via the continuous, controlled injection of oxygen to give a head space partial pressure of 100 kPa. The autoclave contents were sampled as slurry collected after 10, 20, and 30 min reaction time, and every 15 min thereafter; the total reaction time was 90 min for each test. After leaching, the slurries were filtered and the residues were washed, repulped, refiltered, and dried overnight in an oven set at 70 °C. The washed residues and leach solutions were submitted for the elemental analysis by inductively coupled plasma-optical emission spectroscopy (ICP-OES). Sulphur analyses were performed using a LabFit CS-2000 analyser. A selection of residues was submitted for the XRD analysis.

Case Two: Details of the microbial inoculum, the bioreactor setup, sampling, and subsequent analytical methods have been described in Kaksonen *et al.* (2014a, 2014b). Briefly, a two-stage continuous stirred tank reactor (CSTR) system as illustrated in Figure 1 was assembled for iron oxidation and precipitation at room temperature (23 ± 2 °C). A mixed culture of iron oxidizing micro-organisms was applied to assist ferrous oxidation inside the reactors. The influent of the system contained 15 g l^{-1} Fe^{2+} and the pH was adjusted to 1.0, 1.5, 1.9, and 2.2 for each test. Influent was fed with a peristaltic pump into the CSTR1 from which it flowed under gravity to the first settler. The overflow from the first settler was directed by the peristaltic pump to the CSTR2 from which the solution flowed by gravity to the second settler (Figure 1). The effluent

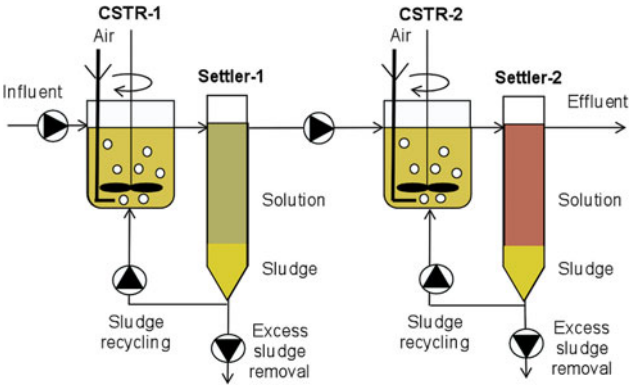

Figure 1. (Color online) Schematic representations for two-stage continuous stirred tank reactor (CSTR) system (Kaksonen *et al.*, 2014a).

from the second settler flowed by gravity to an effluent container. Sludges from settlers 1 and 2 were recycled back into CSTR1 and CSTR2, respectively. Excess sludge was intermittently removed from the settlers using a peristaltic pump. Sludge removed from the settlers was collected to analyse the elemental and mineralogical compositions of the precipitates and for the scanning electron microscopy (SEM). The CSTR influents and effluents were sampled for pH, Fe^{2+}, and soluble Fe analysis.

B. Data collection and analysis for XRD

The mineralogy of the solid samples was examined by the XRD analysis. The XRD traces were obtained after addition of calcium fluoride [CaF_2, to yield 10% (w/w)] as internal standard and micronized in the ethanol medium for 15 min. The micronized sample was air-dried and lightly reground before back-pressing into a conventional XRD sample holder. XRD measurements were carried out using a PANalytical X'Pert PRO diffractometer in Bragg–Brentano geometry equipped with a Co long fine focus tube source operated at 40 kV and 40 mA. The beam path was defined with a 1° divergent, 0.3 mm receiving and 1° anti-scatter slits. A post-diffraction, curved graphite monochromator was used to eliminate $K\beta$ radiation. Patterns were recorded from range of 3 to 140°2θ using a step size of 0.02° and a counting time of 2.5 s per step. Commercially available TOPAS (version 4.2) software (Bruker Advanced X-ray Solutions) was employed to perform the QXRD analysis using the Rietveld method, employing a fundamental parameters approach to line profile fitting for the above instrumental setup.

For the Case One study, all crystalline phases used in the Rietveld refinement were obtained from the ICSD data base using FindIt software, except for nontronite. For this mineral the *hkl* model developed by Wang *et al.* (2012) to account for turbostratic disorder was used. For the Case Two study, the jarosite crystal structure of Menchetti and Sabelli (1976) was used for the QXRD analysis. The proportions of potassium (K^+), sodium (Na^+), ammonium (NH_4^+), and hydronium (H_3O^+) jarosites were calculated based on the K, Na, and N contents of the precipitates, assuming that the jarosite has an ideal composition, and the following relationship between the molar contents of the monovalent cations:

$$[H_3O^+] = 1 - [K^+] - [Na^+] - [NH_4^+] \quad (1)$$

https://doi.org/10.1017/S0885715614001134 Published online by Cambridge University Press

III. RESULTS AND DISCUSSION

A. Case One: Chemistry and mineralogy of feed materials

The chemical and mineralogical compositions of the feed materials used for the Case One study are given in Tables I and II, respectively.

The mineralogical profile of the Bulong laterite deposit consists of a limonite zone with the major minerals goethite and kaolinite, a clay (smectite) zone with mainly nontronite and spinel minerals, and a saprolite zone dominated by antigorite and nontronite (Elias *et al.*, 1981). The major minerals present in the Bulong nickel laterite sample used in the Case One study were nontronite (44%) and goethite (24%), with various minor phases typically present in nickel laterite ores (Table II). Based on the mineralogical analysis, the sample appears to be a blend of limonite and smectite fractions.

The mineralogy of the ore at Poseidon's Mt Windarra deposit has been described by Watmuff (1974). The primary sulphide minerals consist of pentlandite, both monoclinic and hexagonal pyrrhotites, chalcopyrite, and pyrite. Weathering of the primary ore results in gradual replacement of the pentlandite by violarite, and the unviolaritized pyrrhotite may be replaced by secondary pyrite and/or marcasite. QXRD analysis indicates the nickel concentrate used in the present work contains 36% pyrrhotite, 11% pyrite, 7% pentlandite, 7% violarite, and 3% chalcopyrite; as expected the gangue minerals are only minor in quantity (Table II).

B. Case One: Hydrothermal conversion of primary sulphides under HPAL conditions

The change in the compositions of the sulphide minerals in the Poseidon nickel concentrate during oxidative leaching is revealed by the QXRD analysis of the leach residues. The QXRD results are presented in Figures 2(a) (Fe sulphides) and 2(b) (Ni sulphides); the nickel recovery as a function of leaching time is also presented in Figure 2(b). Figure 2(a) indicates that the pyrrhotite in the Poseidon nickel concentrate reacted rapidly, disappearing within the first 10 min, whereas both pyrite and marcasite contents initially increased, and eventually dropped below detection levels within 60 min. This suggests the conversion of pyrrhotite to both pyrite and marcasite. Preferential leaching of marcasite over pyrite was also suggested, with marcasite being completely reacted after 30 min, whereas pyrite was reacted fully after 60 min.

Qian *et al.* (2011) indicated that in the presence of oxygen (O_2) the conversion of pyrrhotite is based on Eq. (2), referred to as the O_2-pathway. The authors suggested that the conversion is a dissolution–reprecipitation replacement process, in which the dissolution of parent pyrrhotite liberates Fe and S, which are necessary for pyrite/marcasite formation. It is worthwhile here indicating that pyrite and marcasite are polymorphs of FeS_2 and are cubic and orthorhombic, respectively. Marcasite formation is favoured over pyrite in initial stages of the conversion, as marcasite requires a lower supersaturation to precipitate than pyrite, while marcasite nucleation is favoured in the presence of pyrrhotite because of the similarity of the mineral structures (Qian *et al.*, 2011).

$$2Fe_{1-x}S_{(s)} + (2-4x)H^{+}_{(aq)} + (1/2-x)O_{2(aq)} \rightarrow FeS_{2(s)} + (1-2x)Fe^{2+}_{(aq)} + (1-2x)H_2O \quad (2)$$

(O_2-pathway)

Pentlandite dissolution also appears to be rapid within the first 20 min [Figure 2(b)]. The violarite content increased slightly during the first 10 min, and gradually decreased below the detection limit by 60 min. This agrees well with the previous finding that Ni and Fe released by dissolution of pentlandite subsequently reprecipitate as violarite based upon Eq. (3) (Xia *et al.*, 2007):

$$(Ni, Fe)_9S_{8(s)} + 1.5O_{2(aq)} + 6H^{+}_{(aq)} \rightarrow 2(Ni, Fe)_3S_{4(s)} + 0.5Ni^{2+}_{(aq)} + 2.5Fe^{2+}_{(aq)} + 3H_2O \quad (3)$$

However, based on the recovery data, only 50% of the nickel reported to solution although the pentlandite was dissolved completely within 20 min [Figure 2(b)]. Given that only ~2% violarite was present at this time, representing only 15% total nickel in the residue, this suggested that the remaining nickel must be present in another solid phase.

During the oxidative leaching of the Poseidon nickel concentrate, new XRD peaks appeared in the 10 min sample, for which the peak intensity reached a maximum after 20 min (Figure 3). Based upon the peak positions the new mineral appears to be similar, but not identical to, vaesite (NiS_2) or bravoite ($Fe_{0.5}Ni_{0.5}S_2$), both of which have a cubic structure ($Pa3$ space group). The formation of this intermediate does not appear to have been previously demonstrated in a hydrothermal environment; however, its formation was predicted by the study of Warner *et al.* (1996) under conditions of increasing oxidation potential. Further study will be required to confirm the formation, chemistry, and crystal structure of this mineral. A cubic NiS_2 structure [gersdorffite; Bayliss and Stephenson (1968)] was used to quantify the concentration of the new intermediate by the QXRD, since it fits the peak positions and relative intensities in the pattern well, as indicated in Figure 3. To explain the formation of this new mineral phase the following equation is proposed, where $0 \leq x \leq 1$:

$$(Ni, Fe)_3S_{4(s)} + 0.5O_{2(aq)} + 2H^{+}_{(aq)} \rightarrow 2(Ni, Fe)S_{2(s)} + xNi^{2+}_{(aq)} + (1-x)Fe^{2+}_{(aq)} + H_2O \quad (4)$$

TABLE I. Chemical composition (wt %) of feed materials used in the Case One study (McDonald *et al.*, 2012).

Elements (%)	Ni	Co	Mg	Mn	Fe	Al	Cr	Si	Na	K	Ca	S
Laterite ore	1.90	0.131	3.32	0.456	24.6	2.47	0.857	16.8	0.201	0.046	0.170	0.02
Sulphide concentrate	8.11	0.138	0.651	0.037	45.0	0.318	0.175	2.48	0.082	0.047	0.421	30.3

https://doi.org/10.1017/S0885715614001134 Published online by Cambridge University Press

TABLE II. Mineralogical composition (w/w %) from QXRD analysis of feed materials used in the Case One study.

Phase (%)	Laterite ore	Sulphide concentrate
Amphibole (actinolite)	0.3	1
Chalcopyrite		3
Chlorite	6	2
Gypsum		0.1
Maghemite/chromite	8	
Magnetite		0.2
Pentlandite		7
Pyrite		11
Pyrrhotite		36
Quartz	4	3
Talc	0.7	3
Vermiculite		0.6
Violarite		7
Goethite	24	
Smectite (nontronite)	44	
Hematite		4
Jarosite/alunite		4
Unaccounted/amorphous	13	19

C. Case One: Iron hydrolysis in HPAL conditions

Dissolution of the Bulong laterite and Poseidon nickel concentrate under oxidative HPAL conditions is expected to produce Fe^{3+} that hydrolyses to generate various precipitate phases depending upon the free acidity of the final leach solutions. According to Umetsu *et al.* (1977) and references therein, at lower acidity (<60 gl^{-1}) and high temperature (200 °C) Fe^{3+} will precipitate as hematite (Fe_2O_3), whereas at high acidity (>60 gl^{-1}) basic ferric sulphate (BFS, $FeOHSO_4$) is formed. At lower temperatures, other basic ferric sulphates such as hydronium jarosite [$MFe_3(SO_4)_2(OH)_6$, where $M = H_3O$] can form and hematite becomes less stable. The formation of jarosites is promoted by the presence of other monovalent cations (M = Na and K) so, even at high temperature and depending upon the prevailing conditions (i.e. M^+ and SO_4^{2-} concentrations), these compounds can form in preference to hematite and BFS (Stoffregen, 1993). Furthermore, if these compounds have aluminium substitution for iron, then the jarosite compound formed is expected to be even more stable (Gaboreau and Vieillard, 2004) and this has also been noted from QXRD analyses of other HPAL residues (Whittington *et al.*, 2003a).

Production of hematite is preferred for optimum acid regeneration and formation of an environmentally preferable residue. The formation of jarosite and BFS are undesirable because of lower acid recovery and potential instability of these materials which can decompose with time to release acid into the environment.

The compositions of the iron precipitation products from the oxidative leaching of Poseidon nickel concentrate [10% (w/w)] are presented in Figure 4(a), whereas for a blend of Poseidon nickel concentrate [10.5% (w/w)] and Bulong laterite ore [19.5% (w/w)] the compositions are shown in Figure 4(b). Hematite was the dominant iron hydrolysis product during the first 30 min of both reactions, increasing to about 50% by the end of the 90 min leaching time. Significant amounts of BFS (26–41%) were found between 45 and 90 min when leaching the Poseidon concentrate; with just under 10% jarosite also present [Figure 4(a)]. This corresponded to increasing acidity after 30 min as a result of sulphide oxidation to sulphuric acid and Fe^{2+} oxidation to Fe^{3+} followed by hematite precipitation. In contrast, only trace amounts of BFS (<2%) and <20% jarosite were present when leaching the blend of the Bulong laterite and Poseidon concentrate [Figure 4(b)]. The presence of laterite in the blend consumes the acid produced resulting in a lower free acidity, ~55 g l^{-1}, which was sufficiently low to inhibit the formation of BFS. As indicated in Section II A, the amount of concentrate blended was calculated to provide sufficient *in situ* acid for the leaching of the laterite ore, minimizing the formation of basic iron sulphate phases.

D. Case Two: Iron oxidation and formation of jarosite in bioreactors

The composition of influent used in the Case Two study is given in Table III. The results of iron oxidation and removal for the two-stage CSTR system are presented in Table IV along with the percentages of copper and nickel loss to the solid precipitates. These results indicate that Fe^{3+} was effectively oxidized for all influent pH values. The percentage of iron removal increased with increasing influent pH, and reached 54% for influent pH 2.2. The percentage of valuable metals (Cu and Ni) lost also increased with increasing influent pH (Table IV).

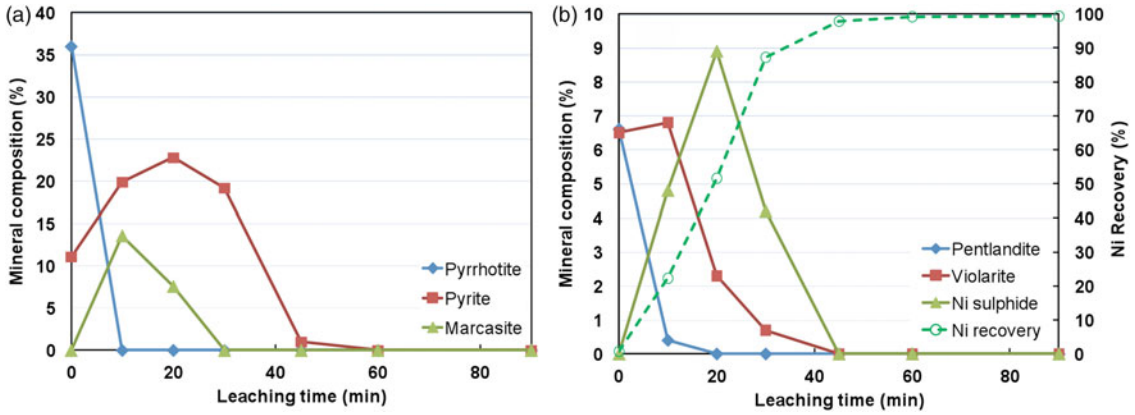

Figure 2. (Color online) Quantitative changes to the contents of the Fe sulphide minerals (a) and the Ni sulphide minerals along with overall Ni recovery (b), from the oxidative leaching of a 10% (w/w) Poseidon nickel concentration as a function of leaching time (modified from McDonald *et al.*, 2012).

https://doi.org/10.1017/S0885715614001134 Published online by Cambridge University Press

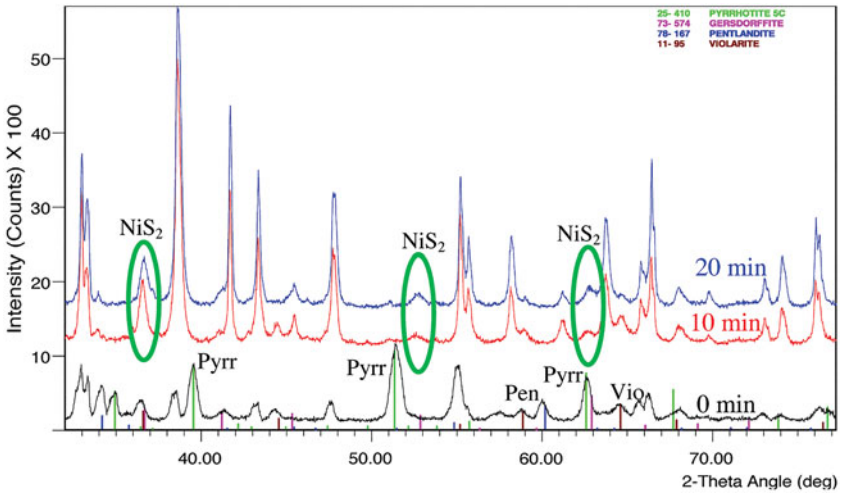

Figure 3. (Color online) XRD patterns of leached residues from the Poseidon nickel concentrate [10% (w/w) pulp density] after 0, 10, and 20 min leaching time, with the oval circles indicating the appearance of new XRD peaks ascribed to a newly formed nickel sulphide with structure similar to vaesite (NiS_2) or bravoite ($(Fe_{0.5}Ni_{0.5}S_2)$). Pyr = pyrrhotite, Pen = pentlandite, and Vio = violarite.

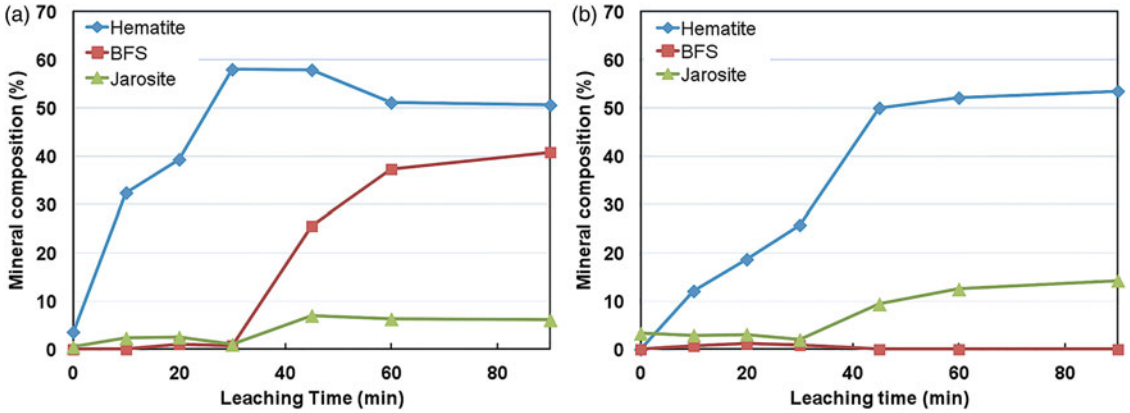

Figure 4. (Color online) Mineralogical compositions of the Fe hydrolysis products from (a) Poseidon nickel concentrate, (b) a blend of Poseidon nickel concentrate [10.5% (w/w)] and Bulong nickel laterite [19.5% (w/w)]. (Modified from McDonald *et al.*, 2012.)

XRD analysis of the precipitates collected from the CSTR1 and 2 indicates that jarosite is the only crystalline mineral present (Figure 5). However, the presence of schwertmannite or other poorly crystalline iron precipitates (e.g. ferrihydrite) cannot be discounted as these may not be readily detected by the XRD when highly crystalline phases are present (i.e. jarosite in this study). In sulphate-containing systems, the formation of schwertmannite is thermodynamically favoured in the pH range of 2–8 (Majzlan *et al.*, 2004). A more recent study (Brand *et al.*, 2013) indicated the possible presence of amorphous material as a precursor to the formation of crystalline natrojarosite. The addition of an internal standard, fluorite, allows the amorphous content of the jarosite precipitate to be calculated from the QXRD analysis by difference. For instance, if the QXRD analysis indicates 97% jarosite with 3% "unaccounted for material", the latter is considered to represent the amorphous content. The purity or the crystallinity of the jarosite is said to be 97%. Using chemical analysis data, the monovalent cation occupancy of the jarosite can also be derived from the QXRD analysis, assuming that all the K, Na, and N (as NH_4^+) present in the sample occupy the same site as H_3O^+ in the jarosite structure. The crystallinity and K occupancy of the jarosite formed in the two stages at different pH are presented in Figures 6(a) and 6(b).

The stability of jarosite analogues is expected to follow the order $K^+ > Na^+ > H_3O^+ > NH_4^+$ from estimates of both heat of formation (Drouet and Navrotsky, 2003) and Gibbs free energy (Gaboreau and Vieillard, 2004). In the present study, given the presence of sufficient potassium, it was expected that K occupancy, which is the molar value of *M* as K in jarosite formula of $MFe_3(SO_4)_2(OH)_6$ (where M = Na, K, and H_3O), would be significant.

The results indicated that the precipitates from CSTR2 contained less impurities compared with those from CSTR1, except at influent pH 2.2 [Figure 6(a)]. The crystallinity of the precipitates increased with increasing influent pH in both

TABLE III. Elemental concentrations of influent used in the Case Two study (Kaksonen *et al.*, 2014a).

Elements	Fe	Cu	Ni	K	Ca	Cl
Influent concentration (g l^{-1})	15	1.5	1.5	0.55	0.1	1

TABLE IV. The percentage of iron oxidation and valuable metals losses from the two-stage CSTR system (Kaksonen *et al.*, 2014a).

pH	Fe^{2+} oxidation (%)	Fe removal (%)	Cu loss (%)	Ni loss (%)
1	99	8.2	0.25	0.01
1.5	99	17	0.61	0.02
1.9	99	43	1.4	0.05
2.2	96	54	2.5	0.26

https://doi.org/10.1017/S0885715614001134 Published online by Cambridge University Press

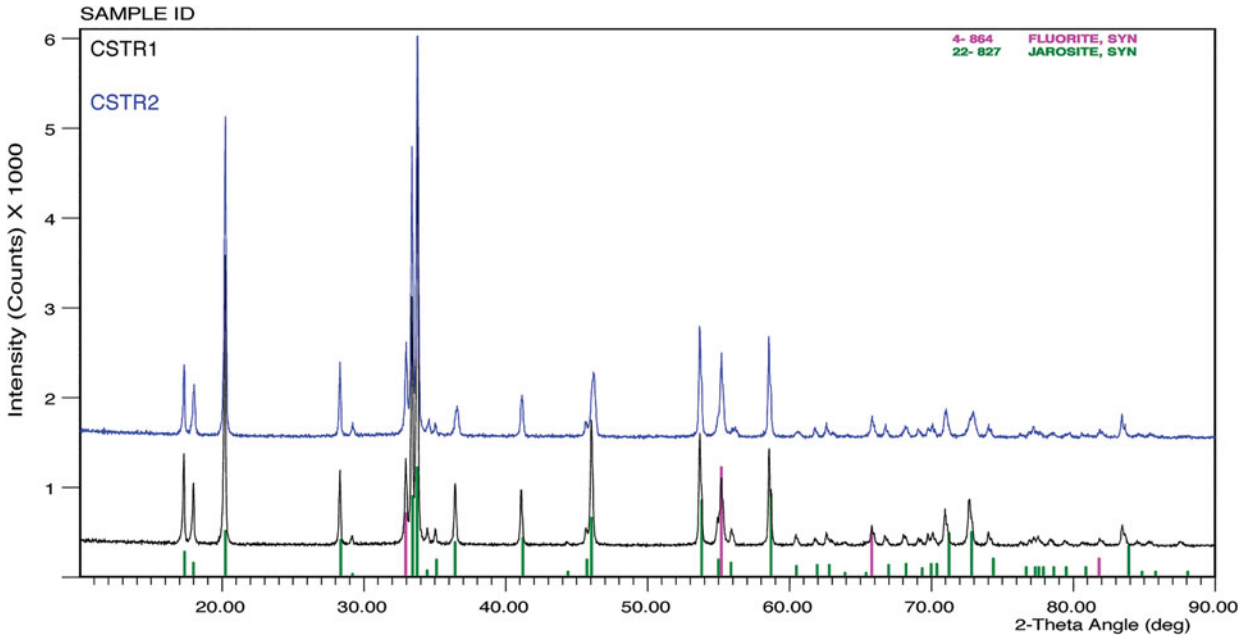

Figure 5. (Color online) XRD of the precipitates collected from CSTR1 and 2 operated at room temperature and influent pH of 1.5; the precipitates were mixed with 10% (w/w) fluorite.

CSTRs, except at pH 2.2. The crystallinity of the precipitate in CSTR2 with influent pH 2.2 actually reduced to ~75%. The reason for this anomaly is unclear. Higher amounts of K^+ were incorporated into jarosite from CSTR1 compared with CSTR2 [Figure 6(b)]. The amount of K^+ incorporation reduced with increasing influent pH in both CSTRs. However, the change was relatively small in CSTR1 (~15% reduced from pH 1.0 to 2.2), but larger in CSTR2 (~70% reduction from pH 1.0 to 2.2) [Figure 6(b)]. Dutrizac and Jambor (2000) indicated that the level of Na^+ incorporated into jarosite was not affected by the change of pH in the range of 0–2, but the amount of jarosite formation reduced from ~90 to 0% when the pH decreased from 2 to 0.5. This explains the near-steady level of K^+ in jarosite from CSTR1. With lower concentrations of K^+ in solution going into CSTR2 and with increasing pH, less K^+ was expected to be incorporated into jarosite from CSTR2.

IV. CONCLUSION

In the Case One study, the hydrothermal conversions of pyrrhotite and pentlandite were demonstrated and quantified using Rietveld-based QXRD analysis and the findings agreed well with previous observations. In addition, a nickel sulphide mineral with cubic structure similar to vaesite and bravoite was identified. Although the leaching of the nickel concentrate produced a significant amount of basic ferric sulphate, the co-processing of nickel laterite and sulphide was shown to generate residues that are more environmentally acceptable. Rietveld-based QXRD analysis can be applied to investigate reaction pathways and specifically the oxidation of sulphide minerals. This may have implications for the geological formation of secondary minerals from primary sulphides. In the Case Two study, QXRD analysis was applied to monitor the solid formation in the bio-processing of iron-containing leach liquors, characterize the mineralogy and crystallinity of the precipitates, and to derive the cation occupancy of the formed jarosites using chemical data.

ACKNOWLEDGEMENTS

The authors acknowledge financial support of CSIRO Mineral Resources Flagship, Vale, Poseidon Nickel, and the Goldfields Esperance Development Council. The authors also thank Barry Halstead (CSIRO Clayton) for collecting the XRD data, and staff in Analytical group in CSIRO Waterford site for chemical analysis of samples discussed in this study.

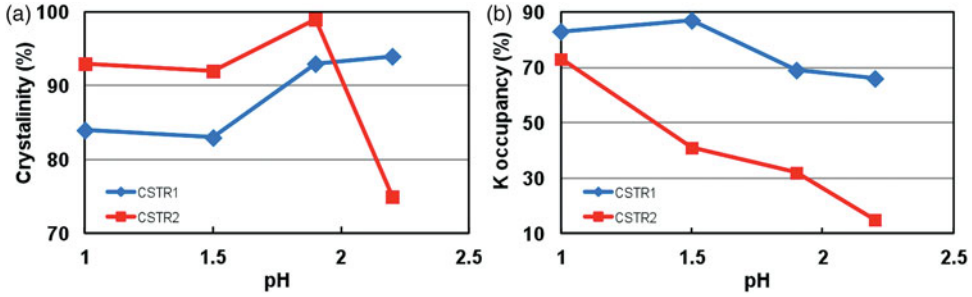

Figure 6. (Color online) Crystallinity of precipitates in CSTR1 and 2 (a) K occupancy of jarosite in CSTR1 and 2 (b) obtained at room temperature.

https://doi.org/10.1017/S0885715614001134 Published online by Cambridge University Press

Bayliss, P. and Stephenson, N. C. (**1968**). "The crystal structure of Gersdorffite (III), a distorted and disordered pyrite structure," Mineral. Mag. **36**, 940–947.

Brand, H. E. A., Scarlett, N. V. Y., Grey, I. E., Knott, R. B., and Kirby, N. (**2013**). "*In situ* SAXS studies of the formation of sodium jarosite," J. Synchrotron Radiat. **20**, 626–634.

Dalvi, A. D., Bacon, W. G., and Osborne, R. C. (**2004**). "The Past and the Future of Nickel Laterites," PDAC 2004 International Convention, Totonto, Canada, March 2004.

Drouet, C. and Navrotsky, A. (**2003**). "Synthesis, characterization and thermochemistry of K–Na–H_3O jarosites," Geochim. Cosmochim. Acta **67**, 2063-2076.

du Plessis, C. A., Slabbert, W., Hallberg, K. B., and Johnson, D. B. (**2011**). "Ferredox: a biohydrometallurgical processing concept for limonitic nickel laterites," Hydrometallurgy **109**, 221–229.

Dutrizac, J. E. and Jambor, J. L. (**2000**). "Jarosites and their application in hydrometallurgy," in *Reviews in Mineralogy and Geochemistry, Volume 40: Sulphate Minerals – Crystallography, Geochemistry and Environmental Significance*, edited by C. N. Alpers, J. L. Jambor and D. K. Nordstrom, (Mineralogical Society of America, Washington) pp. 405–452.

Elias, M., Donaldson, M. J., and Giorgetta, N. E. (**1981**). "Geology, mineralogy, and chemistry of lateritic nickel-cobalt deposits near Kalgoorlie, Western Australia," Econ. Geol. **76**, 1775–1783.

Gaboreau, S. and Vieillard, P. (**2004**). "Prediction of Gibbs free energies of formation of minerals of the alunite supergroup," Geochim. Cosmochim. Acta **68**, 3307–3316.

Geoscience Australia (**2012**). Australia's Identified Mineral Resources, Canberra, ISSN: 1327 1466.

Kaksonen, A. H., Morris, C., Suzy, R., Li, J., Wylie, J., Usher, K. M., Ginige, M. P., Cheng, K. Y., Hilario, F., and du Plessis, C. A. (**2014a**). "Biohydrometallurgical iron oxidation and precipitation: Part I – Effect of pH on process performance," Hydrometallurgy **147–148**, 255–263.

Kaksonen, A. H., Morris, C., Suzy, R., Li, J., Usher, K. M., McDonald, R. G., Hilario, F., Hosken, T., Jackson, M., and du Plessis, C. A. (**2014b**). "Biohydrometallurgical iron oxidation and precipitation: Part II – Jarosite precipitate characterisation and acid recovery by conversion to hematite," Hydrometallurgy **147–148**, 264–272.

Madsen, I. C., Scarlett, N. V. Y., and Whittington, B. I. (**2005**). "Pressure acid leaching of nickel laterite ores: an *in situ* diffraction study of the mechanism and rate of reaction," J. Appl. Crystallogr. **38**, 927–933.

Majzlan, J., Navrotsky, A., and Schwertmann, U. (**2004**). "Thermodynamics of iron oxides: Part III. Enthalpies of formation and stability of ferrihydrite (~$Fe(OH)_3$), schwertmannite (~$FeO(OH)_{3/4}(SO_4)_{1/8}$), and ϵ-Fe_2O_3," Geochim. Cosmochim. Acta **68**, 1049–1059.

McDonald, R., Rodriguez, M., Li, J., Robinson, D., Jackson, M., and Hosken, T. (**2012**). " The co-processing of nickel sulphide and laterite materials using low oxygen pressures," in *Pressure Hydrometallurgy 2012, Proc. of the 42nd Annual Hydrometallurgy Meeting*, edited by M. J. Collins, D. Filippou, J. R. Harlamovs and E. Peek (Niagara Falls, Canada), pp. 211–225.

Menchetti, S. and Sabelli, C. (**1976**). "Crystal chemistry of the alunite series: crystal structure refinement of alunite and synthetic jarosite," Neues Jahrb. Mineral. Monatshefte **1976**, 406–417.

Nurmi, P., Ozkaya, B., Kaksonen, A. H., Tuovinen, O. H., Riekkola-Vanhanen, M. -L., and Puhakka, J. A. (**2009**). "Process for biological oxidation and control of dissolved iron in bioleach liquors," Process Biochem. **44**, 1315–1322.

Ozkaya, B., Sahinkaya, E., Nurmi, P., Kaksonen, A. H., and Puhakka, J. A. (**2007**). "Iron oxidation and precipitation in a simulated heap leaching solution in a *Leptospirillum ferriphilum* dominated biofilm reactor," Hydrometallurgy **88**, 67–74.

Qian, G. Xia, F., Brugger, J., Skinner, W. M., Bei, J., Chen, G., and Pring, A. (**2011**). "Replacement of pyrrhotite by pyrite and marcasite under hydrothermal conditions up to 220°C: an experimental studies of reaction textures and mechanisms," Am. Mineral. **96**, 1878–1893.

Quinn, J., Turner, J. and van der Meulen, D. (**2009**). "The combined pressure acid leach (CPAL) process, batch and piloting testwork, In *Recent Advances in Mineral Processing Plant Design*, edited by D. Malhotra, P. Taylor, E. Spiller and M. LeVier (SME, Littleton, Colorado), pp. 140–154.

Rawlings, D. E. (**2002**). "Heavy metal mining using microbes," Annu. Rev. Microbiol. **56**, 65–91.

Rodriguez, M. (**2009**). "Rheological method for the hydrometallurgical recovery of base metals from ores," World Patent WO2009/149522 A1.

Scarlett, N. V. Y., Madsen, I. C., and Whittington, B. I. (**2008**). "Time-resolved diffraction studies into the pressure acid leaching of nickel laterite ores: a comparison of laboratory and synchrotron X-ray experiments," J. Appl. Crystallogr. **41**, 572–583.

Stoffregen, R. E. (**1993**). "Stability relations of jarosite and natrojarosite at 150–250°C," Geochim. Cosmochim. Acta **57**, 2417–2429.

Umetsu, Y., Tozawa, K. and Sasaki, K. (**1977**). "The hydrolysis of ferric sulphate solutions at elevated temperatures," Can. Metall. Q. **16**, 111–117.

Wang, X., Li, J., Hart, R. D., van Riessen, A., and McDonald, R. (**2011**). "Quantitative X-ray diffraction phase analysis of poorly ordered nontronite clay in nickel laterites," J. Appl. Crystallogr. **44**, 902–910.

Wang, X., Hart, R. D., Li, J., McDonald, R. G., and van Riessen, A. (**2012**). "Quantitative analysis of turbostratically disordered nontronite with a supercell model calibrated by the PONKCS method," J. Appl. Crystallogr. **45**, 1295–1302.

Warner, T. E., Rice, N. M., and Taylor, N. (**1996**). "Thermodynamic stability of pentlandite and violariteand new EH-pH diagrams for the iron-nickel sulphur aqueous system," Hydrometallurgy **41**, 107–118.

Watmuff, I. G. (**1974**). "Supergene alternation of the Mt Windarra nickel sulphide ore deposit, Western Australia," Mineral. Deposita **9**, 199–221.

Wang, X., McDonald, R. G., Hart, R. D., Li, J., and van Riessen, A. (**2014**). "Acid resistance of goethite in nickel laterite ore from Western Australia. Part II. Effect of liberating cementations on acid leaching performance," Hydrometallurgy **140**, 49–58.

Whittington, B. I. and Muir, D. (**2000**). "Pressure acid leaching of nickel laterites: a review," Miner. Process. Extractive Metall. Rev. **21**, 527–600.

Whittington, B. I., McDonald, R. G., Johnson, J. A., and Muir, D. M. (**2003a**). "Pressure acid leaching of arid-region nickel laterite ore. Part I. Effect of water quality," Hydrometallurgy **70**, 31–46.

Whittington, B. I., Johnson, J. A., Quan, L. P., McDonald, R. G., and Muir, D. M. (**2003b**). "Pressure acid leaching of arid-region nickel laterite ore. Part II. Effect of ore type," Hydrometallurgy **70**, 47–62.

Xia, F., Zhou, J., Pring, A., Ngothai, Y., and O'Neill, B. (**2007**). "The role of pyrrhotite (Fe_7S_8) and the sample texture in the hydrothermal transformation of pentlandite ($(Fe,Ni)_9S_8$) to violarite ($(Ni,Fe)_3S_4$)," React. Kinetics Catal. Lett. **92**, 257–266.

https://doi.org/10.1017/S0885715614001134 Published online by Cambridge University Press